Linear and Nonlinear Traveling Edge Waves in Optical Honeycomb Lattices

Mark J. Ablowitz[1], Christopher W. Curtis[2], Yi-Ping Ma[1]
[1] *Department of Applied Mathematics, University of Colorado, Boulder, Colorado 80309, USA*
[2] *Department of Mathematics and Statistics, San Diego State University, San Diego, CA 92182, USA*

Traveling unidirectional localized edge states in optical honeycomb lattices are analytically constructed. They are found in honeycomb arrays of helical waveguides designed to induce a periodic pseudo-magnetic field varying in the direction of propagation. Conditions on whether a given pseudo-field supports a traveling edge mode are discussed; a special case of the pseudo-fields studied agrees with recent experiments. Interesting classes of dispersion relations are obtained. Envelopes of nonlinear edge modes are described by the classical one-dimensional nonlinear Schrödinger equation along the edge. Novel nonlinear states termed edge solitons are predicted analytically and found numerically.

I. INTRODUCTION

Substantial attention has been paid to the understanding of edge modes in both condensed matter physics and optics. Interest in such modes goes back to the first studies of the Quantum Hall Effect (QHE) where it was found that the edge current was quantized [1–3]. There has also been interesting research on the connection of the existence of edge states to the geometry of eigenspaces of Schrödinger operators [4–9]. Recently, theoretical results gave support to the possible existence of unidirectional modes in optical honeycomb lattices [10, 11]. Due to the extra symmetry of the honeycomb lattice, Dirac points, or conical intersections between dispersion bands, exist. The unidirectional modes in [10, 11] emerged due to symmetry breaking perturbations which separated the Dirac points and induced a nontrivial integer "topological" charge on the separated bands.

The first experimental realization of unidirectional electromagnetic edge modes was in [12]. These results relied on magnetic field effects, and were carried out in the microwave regime. Further, the modes were found on a square lattice which have no associated Dirac points. However, in recent work, it was experimentally shown in [13] that by introducing a symmetry breaking pseudo-magnetic field into a honeycomb optical lattice, the Dirac points separate and unidirectional edge wave propagation at optical frequencies occurs. These edge waves are shown to be effectively immune to backscattering from obstacles and so represent a new degree of control of light.

Such psuedo-magnetic fields are generated by a periodic change in the index of refraction of the waveguides in the direction of propagation. Considering the direction of the wave propagation as "time", the variation in the index of refraction has a well defined helicity and thus breaks "time"-reversal symmetry [13]. To model this effect in a honeycomb optical lattice, we begin with the lattice nonlinear Schrödinger (NLS) equation [13] with cubic Kerr contribution

$$i\partial_z\psi = -\frac{1}{2k_0}\nabla^2\psi + \frac{k_0\Delta n}{n_0}\psi - \gamma\left|\psi\right|^2\psi. \qquad (1)$$

Here k_0 is the input wavenumber, n_0 is the ambient refractive index, $\Delta n/n_0$ is the linear index change relative to n_0, also referred to as the potential, and γ represents the nonlinear index contribution. The complex scalar field ψ is the envelope of the electric field, z is the direction of propagation and takes on the role of "time", (x, y) is the transverse plane, and $\nabla \equiv (\partial_x, \partial_y)$. In [13], the potential Δn is taken to be a 2D lattice potential defined on the (x, y)-plane moving along a prescribed path in the z-direction. This motion is characterized by a path function $\mathbf{a}(z) = (a_1(z), a_2(z))$, such that after the coordinate transformation

$$x' = x - a_1(z),\ y' = y - a_2(z),\ z' = z,$$

the transformed potential $\Delta n = \Delta n(x', y')$ is independent of z'.

Experimentally, the path represented by $\mathbf{a}(z)$ can be written into the optical material (e.g. fused silica) via the femtosecond laser writing technique [24], which was the method used in [13]. Since this technique enables waveguides to be written along general paths, we only require $\mathbf{a}(z)$ to be a smooth function. Introducing a transformed field

$$\psi = \tilde{\psi}\exp\left[\frac{i}{2k_0}\int_0^z |\mathbf{A}(\xi)|^2 d\xi\right],$$

where $\mathbf{A}$ is induced by the path function $\mathbf{a}$ via the formula

$$\mathbf{A}(z) = -k_0\mathbf{a}'(z), \qquad (2)$$

we transform Eq. (1) to

$$i\partial_{z'}\tilde{\psi} = -\frac{1}{2k_0}(\nabla' + i\mathbf{A}(z'))^2\tilde{\psi} + \frac{k_0\Delta n}{n_0}\tilde{\psi} - \gamma\left|\tilde{\psi}\right|^2\tilde{\psi}. \qquad (3)$$

In these coordinates, $\mathbf{A}$ appears in the same way as if we had added a magnetic field to Eq. (1), and so we call $\mathbf{A}$ a pseudo-magnetic field. Taking l to be the lattice scale size, we employ the dimensionless coordinates $x' = lx$, $y' = ly$, $z' = 2k_0l^2z$. We introduce the scaled field $\tilde{\psi} = \sqrt{P_*}\psi$, where P_* is input peak power, and by rescaling $\mathbf{A}$ accordingly, and defining $V(\mathbf{r}) = 2k_0^2l^2\Delta n/n_0$ where $\mathbf{r} \equiv (x, y)$, we get the normalized lattice NLS equation

$$i\partial_z\psi = -(\nabla + i\mathbf{A}(z))^2\psi + V(\mathbf{r})\psi - \sigma_0\left|\psi\right|^2\psi. \qquad (4)$$

The dimensionless coefficient $\sigma_0 = 2\gamma k_0 l^2 P_*$ is the strength of the nonlinear change in the index of refraction. We also note that for convenience, the dimensionless variables x, y, z, ψ are used; these dimensionless variables should not be confused with the dimensional variables in Eq. (1). In this paper we take the potential $V(\mathbf{r})$ to be of honeycomb (HC) type.

It is interesting to note that in condensed matter physics Eq. (4) with $\sigma_0 = 0$ describes Bloch electrons in a homogeneous electric field [15], where the electric field is proportional to the time derivative of the vector potential $\mathbf{A}$. Thus, although the parameter regime addressed in this paper is chosen to be consistent with experiments done on optical graphene in [13], the basic asymptotic theory described in this paper applies to different and important physical phenomena.

In [13], in terms of normalized coordinates, the particular helical pseudo-magnetic field

$$\mathbf{A}(z) = (A_1(z), A_2(z)) = \kappa(\sin\Omega z, -\cos\Omega z) \qquad (5)$$

where κ and Ω are constant, was studied numerically and experimentally. Numerically calculated dispersion relations of the associated discrete wave problem, obtained after employing the tight-binding approximation, are given which indicate the existence of unidirectional edge modes. Motivated by the work in [13] and [14], we analytically investigate the existence of unidirectional traveling edge modes. This is done for general periodic pseudo-fields $\mathbf{A}(z)$ which includes Eq. (5) as a subcase. By allowing the pseudo-field to evolve relatively rapidly, which is consistent with the experiments in [13], and by using Floquet theory (cf. [17, 18]), an asymptotic theory is developed which leads to explicit formulae describing how the dispersion relation depends on a given pseudo-field $\mathbf{A}(z)$. Therefore, we can theoretically predict for general pseudo-fields when unidirectional modes exist.

To exemplify the different dispersion relations allowed by our analysis, we generalize the helical motion in Eq. (5) to include one additional trigonometric term

$$\begin{aligned} A_1(z) &= \kappa\sin\Omega z + \lambda\sin(D\Omega z + \phi), \\ A_2(z) &= -\kappa\cos\Omega z + \lambda\cos(D\Omega z + \phi), \end{aligned}$$

where D is taken to be 1 or 2, λ is constant, and we take $\phi = \pi/4$. The values of κ, λ, and ϕ are related to the amplitude of the first harmonic, additional harmonic, and phase offset of the additional harmonic respectively. Since $\mathbf{A}(z)$ is given by Eq. (2), in principle, for every $\mathbf{a}(z)$ written into the the optical lattice, each of the terms κ, λ, and ϕ can be controlled via the laser-writing procedure. Within this extended family of pseudo-fields, we analytically find dispersion relations of the same form that were found in [13] as well as novel classes of dispersion relations. In terms of wave propagation, we find that in addition to nearly unidirectional wave propagation, there are cases with significant dispersion. Thus, not every symmetry-breaking pseudo-field generates coherent unidirectional modes.

We are also able to analyze the effect of nonlinearity on these traveling edge modes. The classical one-dimensional nonlinear Schrödinger equation governing the envelope of the edge modes is derived below and is found to be an effective description of nonlinear traveling edge modes. Using this equation, we find analytically, and confirm numerically, that the unidirectionality of waves is maintained in the in the case of soliton propagation. In the focusing NLS evolution, the nonlinearity balances dispersion to produce nonlinear edge solitons.

Depending on the choice of parameters, some of the nonlinear modes appear to be immune to backscattering, and they are in the topologically protected regime predicted by linear theory cf. [13]. This indicates that unidirectional nonlinear edge modes should be observable. These results hint, for the first time, at a new means for the control of light conferred by merging nonlinear and symmetry-breaking effects. See also [19], where bulk nonlinear modes have been found. Further, such "topologically protected nonlinear states" can apply to other systems; e.g. recently introduced one dimensional domain walls [25].

II. PRELIMINARIES

To begin the analysis, the substitution $\psi = e^{-i\mathbf{r}\cdot\mathbf{A}(z)}\phi$ in Eq. (4) gives

$$i\partial_z\phi = -\Delta\phi - \mathbf{r}\cdot\mathbf{A}_z\phi + V(\mathbf{r})\phi - \sigma_0|\phi^2|\phi. \qquad (6)$$

The tight binding approximation for large V assumes a Bloch wave envelope of the form [21]

$$\phi \sim \sum_{\mathbf{v}} \left(a_{\mathbf{v}}(z)\phi_{1,\mathbf{v}} + b_{\mathbf{v}}(z)\phi_{2,\mathbf{v}}\right) e^{i\mathbf{k}\cdot\mathbf{v}} \qquad (7)$$

where $\phi_{1,\mathbf{v}} = \phi_1(\mathbf{r}-\mathbf{v})$, $\phi_{2,\mathbf{v}} = \phi_2(\mathbf{r}-\mathbf{v})$ are the linearly independent orbitals associated with the two sites A and B where the honeycomb potential $V(\mathbf{r})$ has minima in each fundamental cell, and $\mathbf{k}$ is a vector in the Brillouin zone. Each $\mathbf{v} = m\mathbf{v}_1 + n\mathbf{v}_2$, where the period vectors $\mathbf{v}_1$ and $\mathbf{v}_2$ are given by

$$\mathbf{v}_1 = \left(\sqrt{3}/2,\ 1/2\right),\ \mathbf{v}_2 = \left(\sqrt{3}/2,\ -1/2\right).$$

Fig. 1 shows the semi-infinite honeycomb lattice with zig-zag boundary conditions studied in this paper. The indexing scheme for the A and B sites follows [20]. For each site $\{\mathrm{A},\mathrm{B}\}_{m,n}$, the subscripts m and n denote respectively the infinite and semi-infinite directions. The zig-zag boundary conditions require $n \geq 0$ for $\mathrm{B}_{m,n}$ and $n \geq 1$ for $\mathrm{A}_{m,n}$, while $m \in \mathbb{Z}$ for both. The honeycomb lattice is formed by those sites with $m+n$ even, but to facilitate the computation we carry out the analysis for the entire semi-infinite lattice in the (m,n)-plane. In addition to the primitive lattice vectors $\mathbf{v}_1$ and $\mathbf{v}_2$, Fig. 1 also shows the vectorial distance $\mathbf{d}$ between two adjacent sites $\mathrm{A}_{m,n}$ and $\mathrm{B}_{m,n}$. It can be seen that $\mathbf{d} = (1/\sqrt{3}, 0)$

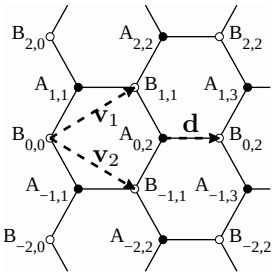

FIG. 1: The semi-infinite honeycomb lattice with zig-zag boundary conditions. The A and B sites are indexed following [20]. The primitive lattice vectors $\mathbf{v}_1$ and $\mathbf{v}_2$, and the inter-site distance $\mathbf{d}$ are also labeled.

for a perfect honeycomb lattice. Substituting the tight binding approximation (7) into Eq. (6), carrying out the requisite calculations (see [21] for more details), and after dropping small terms and renormalizing, we arrive at the following 2D discrete system

$$i\partial_z a_{mn} + e^{i\mathbf{d}\cdot\mathbf{A}}(\mathcal{L}_-(z)b)_{mn} + \sigma|a_{mn}|^2 a_{mn} = 0, \quad (8)$$

$$i\partial_z b_{mn} + e^{-i\mathbf{d}\cdot\mathbf{A}}(\mathcal{L}_+(z)a)_{mn} + \sigma|b_{mn}|^2 b_{mn} = 0, \quad (9)$$

where

$$(\mathcal{L}_- b)_{mn} = b_{mn} + \rho(b_{m-1,n-1}e^{-i\theta_1} + b_{m+1,n-1}e^{-i\theta_2}),$$
$$(\mathcal{L}_+ a)_{mn} = a_{mn} + \rho(a_{m+1,n+1}e^{i\theta_1} + a_{m-1,n+1}e^{i\theta_2}),$$

ρ is a lattice deformation parameter, $\theta_1(z) = \mathbf{v}_1 \cdot (\mathbf{k} + \mathbf{A}(z))$, $\theta_2(z) = \mathbf{v}_2 \cdot (\mathbf{k} + \mathbf{A}(z))$, and σ is a constant which depends on σ_0 and the underlying orbitals. Taking a discrete Fourier transform in m, i.e. letting $a_{mn} = a_n e^{im\omega}$ and $b_{mn} = b_n e^{im\omega}$, yields the simplified system

$$i\partial_z a_n + e^{i\mathbf{d}\cdot\mathbf{A}}\left(b_n + \rho\gamma^*(z;\omega)b_{n-1}\right) + \sigma|a_n|^2 a_n = 0, \quad (10)$$

$$i\partial_z b_n + e^{-i\mathbf{d}\cdot\mathbf{A}}\left(a_n + \rho\gamma(z;\omega)a_{n+1}\right) + \sigma|b_n|^2 b_n = 0, \quad (11)$$

where $\gamma(z;\omega) = 2e^{i\varphi_+(z)}\cos(\varphi_-(z) - \omega)$, with

$$\varphi_+(z) = (\theta_2(z) + \theta_1(z))/2, \ \varphi_-(z) = (\theta_2(z) - \theta_1(z))/2.$$

III. LINEAR THEORY

In this section we omit the nonlinear terms by setting $\sigma = 0$; the nonlinear case is discussed in Section V. The theory we develop is based upon the normalized frequency of the pseudo field being large, which is consistent with the experimental parameters used in [13]. This leads to an analytical formulation in which we can express the linear dispersion relation explicitly in terms of integrals which are readily computed. The details of the asymptotic method are reserved for Appendix A; here we only give the main formulae.

Since we assume that the pseudo magnetic field varies rapidly, we express it as $\mathbf{A} = \mathbf{A}(\zeta)$ where $\zeta = \epsilon^{-1}z, |\epsilon| \ll 1$. Employing the method of multiple-scales [23], we write the vectors a and b as functions of the fast and slow scales, ζ, z, and expand so that the n^{th} components of each vector are given by

$$a_n = a_n(z,\zeta) = a_n^{(0)} + O(\epsilon), \ b_n = b_n(z,\zeta) = b_n^{(0)} + O(\epsilon).$$

We apply zig-zag boundary conditions, which implies $a_n = 0, n \le 0$. The asymptotic method in the Appendix shows that at leading order we have a mode which is nearly stationary; it is given by

$$a_n^{(0)} = 0, \ \ b_n^{(0)} = C(Z)b_n^S, \ b_n^S = \left(-\bar{\vartheta}/\bar{\varrho}\right)^n,$$

where

$$\varrho(\zeta) = e^{i\mathbf{d}\cdot\mathbf{A}}, \quad \vartheta(\zeta;\omega) = \vartheta_c(\zeta)\cos\omega + \vartheta_s(\zeta)\sin\omega,$$
$$\vartheta_c(\zeta) = \varrho(\zeta)\cdot 2\rho e^{-i\varphi_+}\cos\varphi_-,$$
$$\vartheta_s(\zeta) = \varrho(\zeta)\cdot 2\rho e^{-i\varphi_+}\sin\varphi_-,$$

and the average $\bar{f}$ means

$$\bar{f} \equiv T^{-1}\int_0^T f(\zeta)d\zeta,$$

where T is the period of $\mathbf{A}$.

The asymptotic method further yields

$$C(Z) = C(0)\exp\left(-i\tilde{\alpha}(\omega)Z\right), \quad (12)$$

where the dispersion relation $\tilde{\alpha}$ is real and given explicitly as a function of the pseudo-magnetic field $\mathbf{A}(\zeta)$ by

$$\tilde{\alpha}(\omega) = -\frac{i}{T}\int_0^T\int_0^\zeta Q(\zeta';\omega)Q^*(\zeta;\omega)d\zeta' d\zeta, \quad (13)$$

with

$$Q(\zeta;\omega) = -\varrho(\zeta)\frac{\bar{\vartheta}}{\bar{\varrho}} + \vartheta(\zeta;\omega). \quad (14)$$

To have localized modes, we need $|\bar{\vartheta}/\bar{\varrho}| < 1$, namely

$$P(\omega) \equiv |\bar{\vartheta}/\bar{\varrho}|^2 = P_0 + P_c\cos 2\omega + P_s\sin 2\omega < 1, \quad (15)$$

where

$$P_0 = \frac{1}{2}\frac{|\bar{\vartheta}_c|^2 + |\bar{\vartheta}_s|^2}{|\bar{\varrho}|^2},$$
$$P_c = \frac{1}{2}\frac{|\bar{\vartheta}_c|^2 - |\bar{\vartheta}_s|^2}{|\bar{\varrho}|^2},$$
$$P_s = \frac{1}{2}\frac{\bar{\vartheta}_c\bar{\vartheta}_s^* + \bar{\vartheta}_c^*\bar{\vartheta}_s}{|\bar{\varrho}|^2}.$$

The interval of localization $\mathcal{I}$, a subset of the circle $S^1 = \mathbb{R}/(\pi\mathbb{Z})$, can be determined from Eq. (15). There are three qualitatively different scenarios

$$\text{(I)}: \sqrt{P_c^2 + P_s^2} < 1 - P_0, \ P_0 < 1,$$
$$\text{(II)}: \sqrt{P_c^2 + P_s^2} > |P_0 - 1|,$$
$$\text{(III)}: \sqrt{P_c^2 + P_s^2} < P_0 - 1, \ P_0 > 1.$$

In case (II), there are two values of ω determined by $|\bar{\vartheta}/\bar{\varrho}| = 1$, say $\omega_\pm$, at which localized modes delocalize. Thus at $\omega_\pm$, the edge band is emitted from the bulk spectrum, and so $\mathcal{I} = (\omega_-, \omega_+)$. In case (I), $\omega_\pm$ drift apart so that $\mathcal{I} = S^1$, while in case (III) they come together so that $\mathcal{I} = \emptyset$.

Letting $Q(\zeta;\omega) = Q_c(\zeta)\cos\omega + Q_s(\zeta)\sin\omega$, Eq. (13) becomes

$$\tilde{\alpha}(\omega) = \tilde{\alpha}_0 + \tilde{\alpha}_c \cos 2\omega + \tilde{\alpha}_s \sin 2\omega, \tag{16}$$

where one finds directly that the $\tilde{\alpha}_0, \tilde{\alpha}_c$ and $\tilde{\alpha}_s$ can be written in terms of double integrals. It follows from Eq. (16) that the number of times N that $\tilde{\alpha}(\omega)$ crosses $\tilde{\alpha} = 0$ on $\mathcal{I}$ can only be $N = 0$, 1, or 2. For $N = 0$ or $N = 2$, it is possible for edge states to exist in pairs which allow propagation in different directions. In this case, the edge modes are susceptible to dispersion. When $N = 1$, though, because of the unique root of $\tilde{\alpha}$, we expect to find unidirectional edge modes that exhibit essentially no dispersion.

We note that the expressions for the localization interval $\mathcal{I}$ and the dispersion relation $\tilde{\alpha}(\omega)$ are invariant under the constant translations

$$(\omega, \mathbf{A}(\zeta)) \to (\omega + (\mathbf{v}_1 - \mathbf{v}_2)\cdot\bar{\mathbf{A}}/2, \mathbf{A}(\zeta) - \bar{\mathbf{A}}),$$
$$(\mathbf{k}, \mathbf{A}(\zeta)) \to (0, \mathbf{A}(\zeta) + \mathbf{k}),$$

where $\bar{\mathbf{A}}$ is an arbitrary constant 2D vector. Hence without loss of generality we shall consider $\mathbf{A}(\zeta)$ with zero mean and set $\mathbf{k} = 0$ in the following.

In this paper the lattice deformation parameter ρ is taken to be positive. As shown in Appendix B, in the tight-binding limit ρ can be tuned to any positive value by slightly deforming a perfect honeycomb potential. Since both $P(\omega)$ and $\tilde{\alpha}(\omega)$ are proportional to ρ^2, as ρ is decreased with the other parameters fixed, the localization interval $\mathcal{I}$ is broadened and the group velocity $\tilde{\alpha}'(\omega)$ is decreased.

Now let us assume that $\mathbf{A}$ possesses the three-fold symmetry (see Fig. 4(a-c) for examples), i.e.

$$\mathbf{A}(\zeta + 2\pi/3) = R_{\frac{2\pi}{3}}\mathbf{A}(\zeta), \tag{17}$$

where $R_{\frac{2\pi}{3}}$ denotes rotation by $2\pi/3$. As shown in Appendix B, in the tight-binding limit we have the approximation $\mathbf{d} = (1/\sqrt{3}, 0)$ independent of ρ. Using the identities $\mathbf{d} - \mathbf{v}_1 = R^{-1}_{\frac{2\pi}{3}}\mathbf{d}$ and $\mathbf{d} - \mathbf{v}_2 = R_{\frac{2\pi}{3}}\mathbf{d}$, we can simplify the off-diagonal element ϑ of the matrix $\mathcal{L}^-$ as

$$\vartheta(\zeta;\omega) = \rho(e^{-i\omega}\varrho(\zeta_+) + e^{i\omega}\varrho(\zeta_-)), \tag{18}$$

where $\zeta_\pm = \zeta \pm 2\pi/3$. It then follows that

$$\bar{\vartheta}/\bar{\varrho} = \rho(e^{-i\omega} + e^{i\omega}), \tag{19}$$

so the localization interval $\mathcal{I}$ depends only on ρ as

$$\mathcal{I} = \begin{cases} (\cos^{-1}(1/(2\rho)), \pi - \cos^{-1}(1/(2\rho))), & \rho \geq 1/2; \\ S^1, & \rho < 1/2. \end{cases}$$

This expression for $\mathcal{I}$ is identical to the one derived in [20] in the absence of the pseudo-field $\mathbf{A}$.

IV. CLASSIFICATION OF THE DISPERSION RELATION

To make this analysis more concrete, we take the periodic pseudo-field to be

$$\mathbf{A}(\zeta) = \kappa\left(s\left(\zeta\right), -c\left(\zeta\right)\right) + \lambda(s(D\zeta + \phi), c(D\zeta + \phi)).$$

Here, $s(\zeta) = \sin\zeta, c(\zeta) = \cos\zeta$, and $\zeta = z/\epsilon$. Unless otherwise stated, we set $\epsilon = 1.5/(2\pi)$, which is motivated by experiments [13]. This pseudo-field is characterized by three continuous parameters κ, λ, and ϕ, and a discrete parameter $D \in \mathbb{Z}$. It can be seen that $\mathbf{A}(\zeta)$ has a $(D+1)$-fold symmetry; in particular, $\mathbf{A}(\zeta)$ has the three-fold symmetry given by Eq. (17) when $D = 3n - 1$, $n \in \mathbb{Z}$. In the following we fix $\phi = \pi/4$ and explore $D = 2$ and $D = 1$.

Fig. 2 shows the (κ, λ)-plane, hereafter referred to as the phase diagram, partitioned based on our asymptotic theory according to all possible combinations of cases (I,II,III) and $N = 0, 1, 2$, hereafter denoted by (case, N). All six combinations have been found. Fig. 3 shows the full dispersion relations, or Floquet parameters, $\alpha(\omega) = \epsilon\tilde{\alpha}(\omega)$ at representative points (a)-(f) on the (κ, λ)-plane in Fig. 2 computed directly using Eqs. (10–11). The numerical computations are performed using a finite number of lattice sites with zig-zag boundary conditions on both ends. Unless otherwise stated, each vector a and b is defined over 20 lattice sites to allow for sufficient decay. The dark black curves in Fig. 3 show Eq. (16). It can be seen that the asymptotic theory describes the dispersion relation of edge modes almost exactly in all cases studied. Fig. 4 shows the pseudo-field $\mathbf{A}$ with the parameters used in Fig. 3.

The phase diagrams in Fig. 2(i)-(iv) are computed using a three-fold symmetric pseudo-field ($D = 2$). Thus at $\rho = 1$ (Fig. 2(i)), we have case (II) with the localization interval $\mathcal{I} = (\pi/3, 2\pi/3)$. In this case the phase diagram is partitioned into $N = 1$ and $N = 0$ regions. In Fig. 3(a), using a pseudo-field with a single harmonic (Fig. 4(a)) as in [13], we obtain an $N = 1$ dispersion curve with a non-zero slope. This indicates that the linear edge mode propagates as in [13]. In Fig. 3(b), using a pseudo-field with a nonzero second harmonic (Fig. 4(b)), we obtain an $N = 0$ dispersion curve that does not connect between the upper and lower bulk dispersion branches.

At $\rho = 0.4 < 1/2$ (Fig. 2(ii)), we have case (I) with $\mathcal{I} = S^1$. In this case the phase diagram is partitioned into $N = 2$ and $N = 0$ regions. Interestingly, these regions appear to respectively coincide with the $N = 1$ and $N = 0$ regions in the $\rho = 1$ case. In Fig. 3(c) and Fig. 3(d), using the same pseudo-fields as in Fig. 3(a) and Fig. 3(b) respectively, we observe that a pseudo-field with a single harmonic gives $N = 2$, but a nonzero second harmonic results in $N = 0$.

At $1/2 < \rho = 0.6 < 1$ (Fig. 2(iii)), we have case (II) with a broader $\mathcal{I}$ than $\rho = 1$. Compared to $\rho = 1$, the $N = 0$ region remains the same but a neighborhood of the boundary of the $N = 1$ region has turned into an $N = 2$

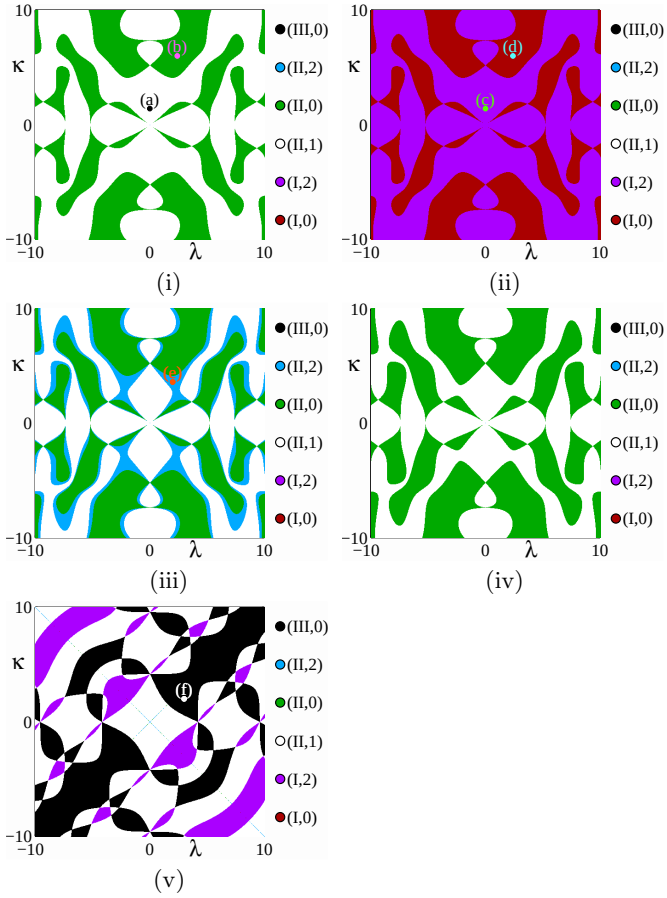

FIG. 2: (Color Online) The (κ, λ)-plane partitioned according to the combinations of cases (I,II,III) and $N = 0, 1, 2$, represented as (case, N) pairs, with parameters (ρ, D): (i) $(1, 2)$; (ii) $(0.4, 2)$; (iii) $(0.6, 2)$; (iv) $(2, 2)$; (v) $(1, 1)$. The full dispersion relations at the labeled points (a)-(f) are shown in Fig. 3.

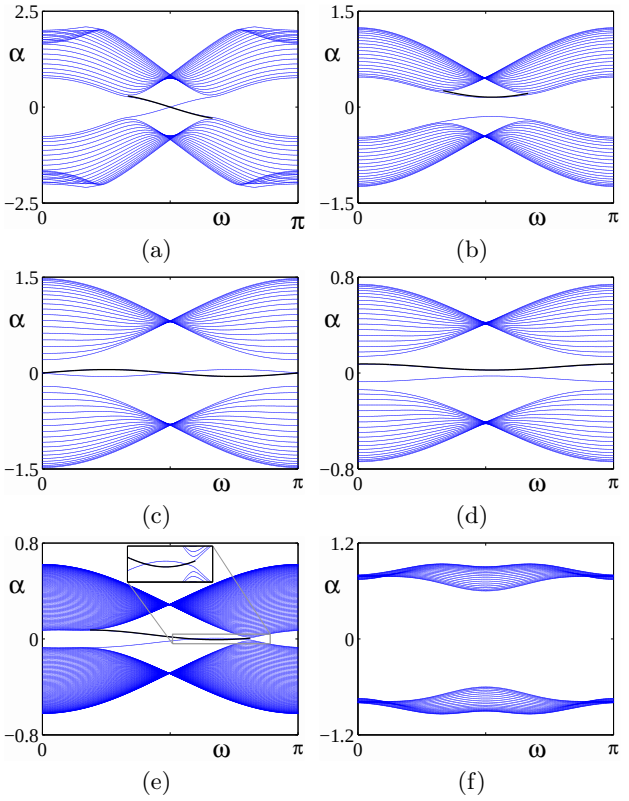

FIG. 3: (Color Online) Dispersion relations for points in Fig. 2 with parameters $(\rho, D, \kappa, \lambda)$: (a) $(1, 2, 1.4, 0)$; (b) $(1, 2, 6, 2.4)$; (c) $(0.4, 2, 1.4, 0)$; (d) $(0.4, 2, 6, 2.4)$; (e) $(0.6, 2, 3.6, 2)$ using 80 lattice sites and $\epsilon = 0.3/(2\pi)$; (f) $(1, 1, 2, 3)$. The black curve shows Eq. (16).

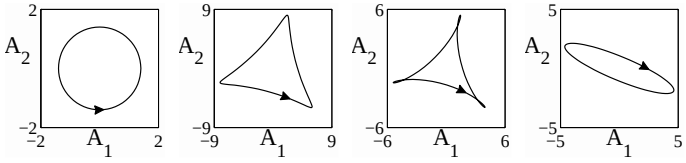

FIG. 4: Plots of the pseudo-field $\mathbf{A}(\zeta) = (A_1(\zeta), A_2(\zeta))$ corresponding to the parameters used in (a) Fig. 3(a,c); (b) Fig. 3(b,d); (c) Fig. 3(e); (d) Fig. 3(f).

region. A typical $N = 2$ dispersion relation computed using the pseudo-field in Fig. 4(c) is shown in Fig. 3(e). Note that in this case, the predicted zero crossing on the right, say ω_r (shown in the inset), is quite close to the predicted value of ω_+. This implies that $P(\omega_r)$ is close to 1 and $\tilde{\alpha}(\omega_+)$ is close to 0. This is a sensitive case, so the number of lattice sites is increased to 80 and ϵ is decreased to $0.3/(2\pi)$. The numerical result is then in good agreement with the asymptotic prediction.

At $\rho = 2 > 1$ (Fig. 2(iv)), we have case (II) with a narrower $\mathcal{I}$ than $\rho = 1$. Compared to $\rho = 1$, the $N = 0$ region has expanded and correspondingly the $N = 1$ region has shrunk.

In the absence of the three-fold symmetry, $\mathcal{I}$ should depend not only on ρ, but also the pseudo-field itself. Fig. 2(v) shows a phase diagram computed using a two-fold symmetric (or elliptic) pseudo-field ($D = 1$). Indeed at $\rho = 1$, we have coexistence between cases (I), (II) and (III). Interestingly, we find only $N = 2$ in the case (I) region and $N = 1$ in the case (II) region. A typical case (III) dispersion relation computed using the pseudo-field in Fig. 4(d) is shown in Fig. 3(f).

We note that the difference between the $N = 1$ and $N = 0, 2$ cases is distinguished by introducing a $\mathbb{Z}_2$ topological index, see [22], $I \equiv N (\mathrm{mod}\, 2)$, such that the former (latter) situation corresponds to $I = 1$ ($I = 0$), namely nontrivial (trivial) topology. We will explore this connection further in the future.

V. NONLINEAR TWO-DIMENSIONAL LOCALIZED EDGE MODES

Following the approach in [20] and to compare with experiments in [13], we construct two-dimensional (2D) localized solutions by introducing an envelope in ω and taking the inverse Fourier transform in m. First we focus on fixed ω and modify our preceding analysis in Sec. III to account for weak nonlinearity where $\sigma = \epsilon\tilde{\sigma}$. The analysis proceeds as before except that r_+ is replaced by $r_+ - \tilde{\sigma}|b^{(0)}|^2 b^{(0)}$ in Eq. (A1). In this case we arrive at the following equation

$$i\partial_Z C = \tilde{\alpha}(\omega)C - \tilde{\sigma}\alpha_{nl}(\omega)|C|^2 C, \tag{20}$$

where $\alpha_{nl}(\omega) = \|b^S\|_4^4/\|b^S\|_2^2$ with

$$\left|\left|b^S\right|\right|_2^2 = \sum_{n=0}^{\infty}\left|b_n^S\right|^2, \quad \left|\left|b^S\right|\right|_4^4 = \sum_{n=0}^{\infty}\left|b_n^S\right|^4.$$

We can reconstruct the approximation to b_{mn} via

$$b_{mn} = C(Z,\omega)e^{i\omega m}b_n^S. \tag{21}$$

In the narrow band approximation with ω near any given $\omega_0 \in \mathcal{I}$, the solution C represents an envelope function with carrier wavenumber ω_0. To describe its dynamics, we first expand $\tilde{\alpha}(\omega)$ and $\alpha_{nl}(\omega)$ around ω_0. We then replace $\omega - \omega_0$ by $-i\nu\partial_y$, where ν is the width around ω_0, or the inverse width of the envelope in physical space. Finally, we rewrite Eq. (20) as the following equation for the envelope C

$$\begin{aligned} i\partial_Z C = &\left[\sum_{j=0}^{3}\frac{\tilde{\alpha}^{(j)}(\omega_0)}{j!}(-i\nu\partial_y)^j + O(\nu^4)\right]C \\ &- \tilde{\sigma}\left[\alpha_{nl}(\omega_0) + O(\nu)\right]|C|^2 C, \end{aligned} \tag{22}$$

where $\tilde{\alpha}^{(j)}(\omega_0)$ denotes the j-th derivative of $\tilde{\alpha}(\omega)$ at $\omega = \omega_0$. Equation (22) is a higher order nonlinear Schrödinger (NLS) equation.

There are interesting subcases. If $\tilde{\alpha}''(\omega_0) \neq 0$, then the equation is reduced at leading order to the well-known NLS equation given below

$$i\partial_{\tilde{Z}}\tilde{C} + \frac{\tilde{\alpha}''(\omega_0)}{2}\tilde{C}_{YY} + \sigma_{eff}|\tilde{C}|^2\tilde{C} = 0, \tag{23}$$

where $C = \tilde{C}(Y,\tilde{Z})e^{-i\tilde{\alpha}(\omega_0)Z}$, $Y = y - \nu\tilde{\alpha}'(\omega_0)Z$, $\tilde{Z} = \nu^2 Z$, and $\sigma_{eff} = \tilde{\sigma}\alpha_{nl}(\omega_0)/\nu^2$. On the other hand if $\tilde{\alpha}''(\omega_0) = 0$ then the following "zero dispersion" NLS equation is obtained

$$i\partial_{Z_3}\tilde{C} - i\frac{\tilde{\alpha}'''(\omega_0)}{6}\tilde{C}_{YYY} + \sigma_{zeff}|\tilde{C}|^2\tilde{C} = 0, \tag{24}$$

where now $C = \tilde{C}(Y,Z_3)e^{-i\tilde{\alpha}(\omega_0)Z}$, $Y = y - \nu\tilde{\alpha}'(\omega_0)Z$, $Z_3 = \nu^3 Z$, and $\sigma_{zeff} = \tilde{\sigma}\alpha_{nl}(\omega_0)/\nu^3$.

As indicated above, Eq. (23) is the classical 1D NLS equation. The equation is maximally balanced when $\sigma_{eff} = O(1)$. In the focusing case, $\tilde{\alpha}''(\omega_0)\sigma_{eff} > 0$, the NLS equation is known to contain solitons. Thus in this case the semi-infinite HC lattice truly contains edge solitons. In the defocusing case, $\tilde{\alpha}''(\omega_0)\sigma_{eff} < 0$, the nonlinearity enhances dispersion, and so no soliton is expected. For the zero-dispersion NLS equation (24), which applies when $\tilde{\alpha}''(\omega_0) = 0$ and $\sigma_{zeff} = O(1)$, the nonlinearity also enhances dispersion somewhat.

To test these predictions, we solve the 2D discrete system Eqs. (8–9) numerically using the initial condition

$$a_{mn} = 0, \quad b_{mn} = \int_{\mathcal{I}}\hat{b}(\omega)\frac{b_n^S(\omega)}{\sqrt{\langle b^S(\omega), b^S(\omega)\rangle}}e^{im\omega}d\omega, \tag{25}$$

where

$$\hat{b}(\omega) = \frac{e^{-(\omega-\omega_0)^2/\nu^2}}{\int_{\mathcal{I}}e^{-(\omega-\omega_0)^2/\nu^2}d\omega},$$

and compare the results with b_{mn} reconstructed from numerical solutions of the 1D NLS equation (22) with the initial condition

$$C(Z=0,y) = \int_{\mathcal{I}}\hat{b}(\omega)\frac{1}{\sqrt{\langle b^S(\omega), b^S(\omega)\rangle}}e^{iy(\omega-\omega_0)/\nu}d\omega. \tag{26}$$

In Fig. 5, we compare linear ($\sigma = 0$) edge modes found from the full 2D discrete system to those found from the 1D linear Schrödinger (LS) equation, i.e. Eq. (22) with $\tilde{\sigma} = 0$. The comparison of results is shown in terms of $|b_{m0}(z)|$. The left panels (a,c,e) show the solutions of the 2D discrete system and the right panels (b,d,f) show the solutions of the 1D LS equation where we use the following modification of Eq. (21),

$$b_{mn} = C(Z,y)e^{i\omega_0 y/\nu}b_n^S, \tag{27}$$

to reconstruct b_{mn} with C satisfying the LS equation.

In Fig. 6, we compare nonlinear ($\sigma \neq 0$) edge modes found from the full 2D discrete system to those found from the full 1D NLS equation (22). As before, the comparison of results is shown in terms of $|b_{m0}(z)|$, the left panels (a,c,e) show the solutions of the 2D discrete system and the right panels (b,d,f) show the solutions of the 1D NLS equation with Eq. (27) used to reconstruct $|b_{m0}(z)|$.

In the absence of nonlinearity ($\sigma = 0$), the fastest and most robust unidirectional traveling mode is seen in Fig. 5(a), which corresponds to the $N = 1$ dispersion curve in Fig. 3(a) with $\tilde{\alpha}'(\omega_0) \neq 0$ [13]. In this case, relatively weak dispersion results from $\tilde{\alpha}''(\omega_0) = 0$ and the term $\tilde{\alpha}'''(\omega_0) \neq 0$ is a small higher order contribution. Figs. 5(c) and 5(e) both correspond to the $N = 2$ dispersion curve in Fig. 3(c) with $\tilde{\alpha}'(\omega_0) = 0$. In both cases, the linear dispersion resulting from $\tilde{\alpha}''(\omega_0) \neq 0$ essentially eliminates the mode after sufficient evolution.

Fig. 6(a) shows the nonlinear evolution using the same parameters as Fig. 5(a) but with $\sigma = 0.005 \sim \epsilon\nu^3$. Comparing these two panels, we see that the unidirectional

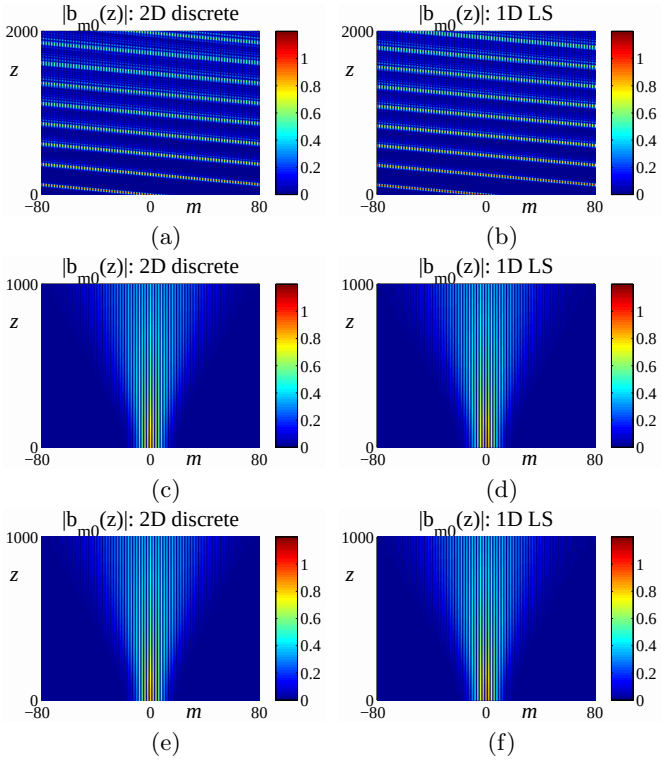

FIG. 5: (Color Online) Plot of $|b_{m0}(z)|$ (at the edge) for parameters (ρ, ν, ω_0): (a,b) $(1, 0.2, \pi/2)$; (c,d) $(0.4, 0.2, \pi/4)$; (e,f) $(0.4, 0.2, 3\pi/4)$. The pseudo-field parameters are fixed at $(D, \kappa, \lambda) = (2, 1.4, 0)$, and the edge modes are linear ($\sigma = 0$). Periodic boundary conditions in m are used. The left panels are calculated from the 2D discrete system Eqs. (8–9); the right panels are found from the 1D LS equation (22).

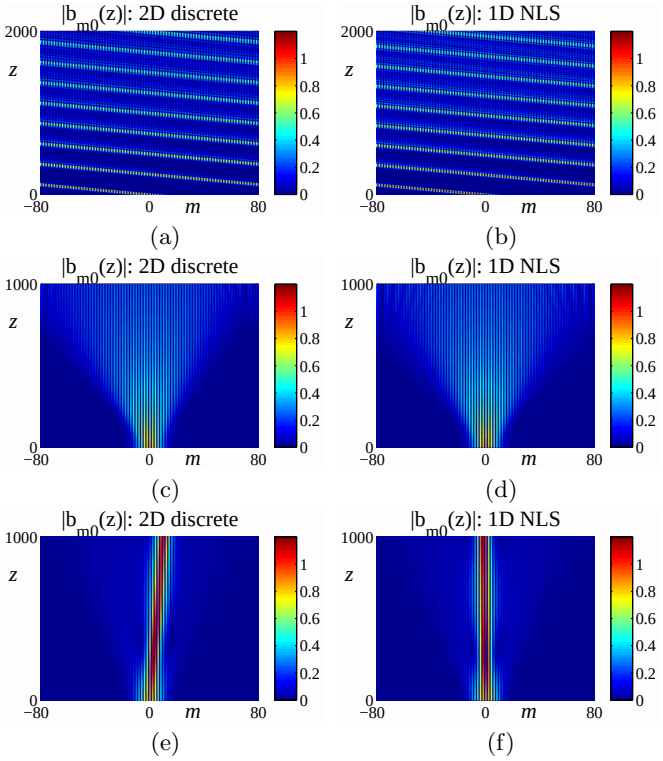

FIG. 6: (Color Online) Plot of $|b_{m0}(z)|$ (at the edge) for the same parameters as Fig. 5 except that (a,b) $\sigma = 0.005$; (c,d,e,f) $\sigma = 0.02$. The left panels are calculated from the 2D discrete system Eqs. (8–9); the right panels are found from the full 1D NLS equation (22) with $\tilde{\sigma} \neq 0$.

traveling mode is largely maintained in the presence of weak nonlinearity, though dispersion is somewhat enhanced in the nonlinear case. Figs. 6(c) and 6(e) show the nonlinear evolutions using the same parameters as in Figs. 5(c) and 5(e) but with $\sigma = 0.02 \sim \epsilon\nu^2$. For Fig. 6(c), which is described by the defocusing NLS equation, which has no solitons due to $\tilde{\alpha}''(\omega_0) < 0$, we see that weak nonlinearity enhances dispersion. On the other hand, for Fig. 6(e), which is described by the focusing NLS equation, which has solitons due to $\tilde{\alpha}''(\omega_0) > 0$, we see that weak nonlinearity enhances localization.

Comparing panels (b,d,f) with panels (a,c,e) in Figs. 5 and 6, we see that the 1D LS/NLS equation (22) reproduces the time evolution of the 2D discrete system (8–9) well up to $z \sim 1/(\epsilon\nu^3)$ for panel (a) and $z \sim 1/(\epsilon\nu^2)$ for panels (c,e). Beyond these time scales, higher-order terms must be added to Eq. (22) in order to explain for example the slow rightward drift of the wave envelope in Fig. 6(e).

Since solitons in the 1D focusing NLS equation are known to be stable, it is interesting to see how the edge solitons found above in the 2D discrete system propagate over long distances. Fig. 7 shows two time evolutions computed using the same parameters as in Fig. 6(e) except that $\omega_0 = 5\pi/8$, and $\rho = 0.6$ for panel (a) and $\rho = 0.4$ for panel (b). Since $\tilde{\alpha}(\omega) \propto \rho^2$, it can be seen from Fig. 3(c) that locally $\tilde{\alpha}'(\omega_0) \neq 0$ and $\tilde{\alpha}''(\omega_0) > 0$ in both cases, and so the governing 1D NLS equation is focusing. The difference between these two choices of ρ is that globally the dispersion relation $\tilde{\alpha}(\omega)$ is topologically nontrivial (case (II), $N = 1$) for $\rho > 1/2$ and topologically trivial (case (I), $N = 2$) for $\rho < 1/2$. Over the distance $z \sim 1/(\epsilon\nu^2)$, the localized wave envelope indeed evolves into a traveling edge soliton in both cases as predicted by the NLS equation. However, for larger z, the edge soliton travels at a uniform velocity in Fig. 7(a), but gradually slows down due to backscattering in Fig. 7(b). This dramatic difference may be attributed to the fact that the linear topologically protected traveling edge waves, which are immune to backscattering, confer this immunity to nonlinear modes, such as the one in Fig. 7(a).

This immunity of traveling edge waves to backscattering in the topologically protected regime is usually explained in terms of the absence of counter-propagating edge modes. For this reason, these edge waves are also

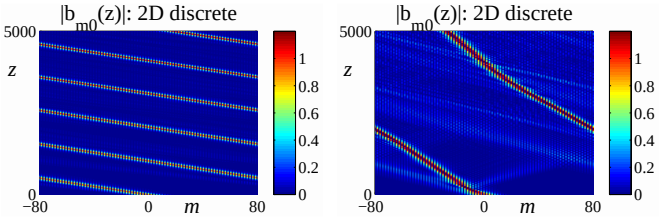

FIG. 7: (Color Online) Plot of $|b_{m0}(z)|$ (at the edge) for the same parameters as Fig. 6(e) except that $\omega_0 = 5\pi/8$, and (a) $\rho = 0.6$; (b) $\rho = 0.4$.

expected to be immune to backscattering, and so maintain their topological protection, in the presence of various types of disorder, at least for a degree of disorder below a certain threshold [7]. A detailed investigation of the dynamical behavior of traveling edge waves, using various types of disordered honeycomb lattices cf. [16] is a topic of interest but is outside the scope of the present study.

VI. CONCLUSION

In this paper, a method is developed which describes the propagation of edge modes in a semi-infinite honeycomb lattice in the presence of a periodically and relatively fast varying pseudo-field and weak nonlinearity. In the linear case, various pseudo-fields are explored, and different dispersion relations are found to occur, some of which exhibit unidirectional wave propagation. A special case agrees with the results and experiments of [13]. With weak nonlinearity included, it is shown that in the narrow band approximation, a higher order NLS equation is obtained. Special cases include the classical NLS and zero dispersion NLS equations. The classical NLS equation admits solitons, and they are found to be part of the long time nonlinear evolution under suitable circumstances. This shows the existence of true edge solitons. Finally, over very long distances, with certain choices of parameters, consistent with the notion of topological protection as indicated by the linear dispersion relation, localized nonlinear edge modes are found to be immune from backscattering, while with other choices of parameters, backscattering is observed.

ACKNOWLEDGEMENTS

This research was partially supported by the U.S. Air Force Office of Scientific Research, under grant FA9550-12-1-0207 and by the NSF under grants DMS-1310200, CHE 1125935.

Appendix A: Asymptotic analysis

With the method of multiple-scales, we write the n^{th} components of the vectors a and b as

$$a_n = a_n(z,\zeta),\ b_n = b_n(z,\zeta).$$

The coupled system given by Eqs. (10–11) then becomes

$$i\epsilon^{-1}\partial_\zeta a + i\partial_z a + \mathcal{L}^-(\zeta;\omega)b = 0,$$
$$i\epsilon^{-1}\partial_\zeta b + i\partial_z b + \mathcal{L}^+(\zeta;\omega)a = 0,$$

where the n^{th} component of $\mathcal{L}^-(\zeta;\omega)b$ is

$$\left(\mathcal{L}^-(\zeta;\omega)b\right)_n = \varrho(\zeta)b_n + \vartheta(\zeta;\omega)b_{n-1},$$

the operator $\mathcal{L}^+$ is the hermitian conjugate of $\mathcal{L}^-$, and

$$\varrho(\zeta) = e^{i\mathbf{d}\cdot\mathbf{A}},\quad \vartheta(\zeta;\omega) = \vartheta_c(\zeta)\cos\omega + \vartheta_s(\zeta)\sin\omega,$$
$$\vartheta_c(\zeta) = \varrho(\zeta)\cdot 2\rho e^{-i\varphi_+}\cos\varphi_-,$$
$$\vartheta_s(\zeta) = \varrho(\zeta)\cdot 2\rho e^{-i\varphi_+}\sin\varphi_-.$$

Then we expand a_n, b_n in powers of ϵ

$$a_n = a_n^{(0)} + \epsilon a_n^{(1)} + \cdots,\ b_n = b_n^{(0)} + \epsilon b_n^{(1)} + \cdots.$$

At $O(\epsilon^{-1})$, $\partial_\zeta a_n^{(0)} = 0$ and $\partial_\zeta b_n^{(0)} = 0$ which leads to $a_n^{(0)} = a_n^{(0)}(z)$ and $b_n^{(0)} = b_n^{(0)}(z)$.

At $O(1)$, to remove secularities, using the average $\bar{f} \equiv T^{-1}\int_0^T f(\zeta)d\zeta$, where T is the period of $\mathbf{A}$, we get

$$i\partial_z a^{(0)} + \bar{\mathcal{L}}^-(\omega)b^{(0)} = \epsilon r_-,\quad i\partial_z b^{(0)} + \bar{\mathcal{L}}^+(\omega)a^{(0)} = \epsilon r_+, \tag{A1}$$

where

$$r_- = -i\overline{\partial_z a^{(1)}} - \overline{\mathcal{L}^-(\zeta;\omega)b^{(1)}},\ r_+ = -i\overline{\partial_z b^{(1)}} - \overline{\mathcal{L}^+(\zeta;\omega)a^{(1)}}, \tag{A2}$$

and where $a^{(1)}$ and $b^{(1)}$ are found from

$$i\partial_\zeta a^{(1)} + (\mathcal{L}^-(\zeta;\omega) - \bar{\mathcal{L}}^-(\omega))b^{(0)} = 0, \tag{A3}$$
$$i\partial_\zeta b^{(1)} + (\mathcal{L}^+(\zeta;\omega) - \bar{\mathcal{L}}^+(\omega))a^{(0)} = 0. \tag{A4}$$

The zig-zag boundary conditions imply $a_n(z,\zeta) = 0, n \le 0$. As $\epsilon \to 0$, we have a stationary mode on the z-scale, so that $a_n^{(0)} = 0$ and $\overline{\mathcal{L}^-(\omega)}b^{(0)} = 0$. Thus to maintain asymptotic balance, for $\epsilon \neq 0$, this mode evolves on the Z-scale where $Z = \epsilon z$, namely

$$b^{(0)} = C(Z)b^S,\ b_n^S = \left(-\bar{\vartheta}/\bar{\varrho}\right)^n.$$

To eliminate secularities at the next order, we must have

$$iC^{-1}\partial_Z C = \langle r_+, b^S\rangle / \langle b^S, b^S\rangle \equiv \tilde{\alpha}, \tag{A5}$$

where $\langle\cdot,\cdot\rangle$ is the inner product between two vectors, and r_+ is evaluated using Eqs. (A2–A4) with $a^{(0)} = 0$ and $b^{(0)} = b^S$. After introducing

$$Q(\zeta;\omega) \equiv \frac{\left(\mathcal{L}^-(\zeta;\omega)b^S\right)_n}{b_{n-1}^S} = -\varrho(\zeta)\frac{\bar{\vartheta}}{\bar{\varrho}} + \vartheta(\zeta;\omega), \tag{A6}$$

we see that $\tilde{\alpha}(\omega)$ becomes

$$\tilde{\alpha}(\omega) = -\frac{i}{T}\int_0^T \int_0^\zeta Q(\zeta^{'};\omega)Q^*(\zeta;\omega)d\zeta^{'}d\zeta. \quad \text{(A7)}$$

From Eq. (A6) we see that $\bar{Q} = 0$; using this fact it is shown in Appendix C that $\tilde{\alpha}$ is strictly real. Therefore the solution to Eq. (A5)

$$C(Z) = C(0)\exp\left(-i\tilde{\alpha}(\omega)Z\right) \quad \text{(A8)}$$

shows that the influence of the nontrivial pseudo-magnetic field $\mathbf{A}(\zeta)$ on the stationary edge modes is the introduction of a non-trivial phase; as mentioned in Section III the function $\tilde{\alpha}(\omega)$ is identified as the dispersion relation.

Appendix B: Relation between the deformation parameter and the honeycomb potential

In this section, we study the dependence of the deformation parameter ρ on the honeycomb potential. The prototypical honeycomb potential used in this paper is (cf. Eq. (2) in [21])

$$V(\mathbf{r}) = V_0\left[\frac{|e^{ik_0\mathbf{b}_1\cdot\mathbf{r}} + \eta e^{ik_0\mathbf{b}_2\cdot\mathbf{r}} + \eta e^{ik_0\mathbf{b}_3\cdot\mathbf{r}}|^2}{(1+2\eta)^2} - 1\right], \quad \text{(B1)}$$

where $\mathbf{b}_1 = (0,1)$, $\mathbf{b}_2 = (-\frac{\sqrt{3}}{2}, -\frac{1}{2})$, $\mathbf{b}_3 = (\frac{\sqrt{3}}{2}, -\frac{1}{2})$, $V_0 > 0$ is the potential strength, and η measures the relative strength of the second and third plane waves. To form a honeycomb lattice, $\eta > \frac{1}{2}$ must be satisfied; $\eta = 1$ corresponds to perfect honeycomb.

In the Appendix to [21], the deformation parameter ρ is expressed in terms of the shift vectors $\mathbf{d}_s$, $s = 0, 1, 2$, from its three nearest B site to an A site. The vectors $\mathbf{d}_s$ are functions of η; the vector $-\mathbf{d}_0$ is denoted by $\mathbf{d}$ in this paper. Near $\eta = 1$, the expression for ρ is, to leading order

$$\rho = e^{\frac{9+\sqrt{3}\pi}{18}\sqrt{V_0}(\eta-1)}, \quad \text{(B2)}$$

which can be solved as

$$\eta - 1 = \frac{18}{9+\sqrt{3}\pi}V_0^{-1/2}\log\rho. \quad \text{(B3)}$$

Near $\eta = 1$, the vector $\mathbf{d}$ becomes, to leading order

$$\mathbf{d} = \left(\frac{1}{\sqrt{3}} + \frac{1}{\pi}(\eta-1), 0\right). \quad \text{(B4)}$$

Therefore, when V_0 is large, as long as ρ is positive and not small, $\mathbf{d}$ changes little as a function of ρ.

Appendix C: The reality of the dispersion relation

To show that $\bar{Q} = 0$ implies that $\tilde{\alpha}(\omega)$ given in Eq. (13) is real, we note that (parametric dependence of Q on ω is omitted for notational convenience)

$$\begin{aligned}
&T\left[i\tilde{\alpha}(\omega) + (i\tilde{\alpha}(\omega))^*\right] \\
&= \int_0^T\int_0^\zeta Q(\zeta')Q^*(\zeta)d\zeta'd\zeta + \int_0^T\int_0^\zeta Q^*(\zeta')Q(\zeta)d\zeta'd\zeta \\
&= \int_0^T\int_0^\zeta Q(\zeta')Q^*(\zeta)d\zeta'd\zeta + \int_0^T\int_\zeta^T Q^*(\zeta)Q(\zeta')d\zeta'd\zeta \\
&= \int_0^T\int_0^T Q(\zeta')Q^*(\zeta)d\zeta'd\zeta = \left|\int_0^T Q(\zeta)d\zeta\right|^2 = 0.
\end{aligned}$$

[1] K. Klitzing, G. Dorda, and M. Pepper. *Phys. Rev. Lett.*, 45:494–497, 1980.
[2] R.B. Laughlin. *Phys. Rev. B*, 23:5632–5633, 1981.
[3] D.J. Thouless, M. Kohmoto, M.P. Nightingale, and M. den Nijs. *Phys. Rev. Lett.*, 49:405–408, 1982.
[4] B. Simon. *Phys. Rev. Lett.*, 51:2167–2170, 1983.
[5] A. Bohm, A. Mostafazadeh, H. Koizumi, Q. Niu, and J. Zwanziger. *The Geometric Phase in Quantum Systems*. Springer, Heidelberg, 2003.
[6] Y. Hatsugai. *Phys. Rev. B*, 48:11851, 1993.
[7] M.Z. Hasan and C.L. Kane. *Rev. Mod. Phys.*, 82:3045–3067, 2010.
[8] D. Xiao, M.C. Chang, and Q. Niu. *Rev. Mod. Phys.*, 82:1959–2007, 2010.
[9] J. Zak. *Phys. Rev. Lett.*, 62:2747–2750, 1989.
[10] F.D.M Haldane and S. Raghu. *Phys. Rev. Lett.*, 100:013904, 2008.
[11] S. Raghu and F.D.M Haldane. *Phys. Rev. A*, 78:033834, 2008.
[12] Z. Wang, Y. Chong, J.D. Joannopoulos, and M. Soljacic. *Nature*, 461:772–776, 2009.
[13] M.C. Rechtsman, J.M. Zeuner, Y. Plotnik, Y. Lumer, S. Nolte, F. Dreisow, M. Segev, and A. Szameit. *Nature*, 496:196–200, 2013.
[14] M.C. Rechtsman, Y. Plotnik, J.M. Zeuner, D. Song,Z. Chen,A. Szameit, and M. Segev. *Phys. Rev. Lett.*, 111:103901, 2013.
[15] J. B. Krieger and G. J. Iafrate. *Phys. Rev. B*, 33:5494, 1986.
[16] M. A. Kaliteevski, J. Manzanares Martinez, D. Cassagne, and J. P. Albert. *Phys. Rev. B*, 66:113101, 2002.
[17] T. Kitagawa, E. Berg, M. Rudner, and E. Demler. *Phys. Rev. B*, 82:235114, 2010.
[18] N. H. Lindner, G. Refael, and V. Galitski. *Nature Physics*, 7:490–495, 2011.
[19] Y. Lumer, Y. Plotnik, M.C. Rechtsman, and M. Segev. *Phys. Rev. Lett.*, 111:243905, 2013.
[20] M.J. Ablowitz, C.W. Curtis, and Y. Zhu. *Phys. Rev. A*, 88:013850, 2013.
[21] M. J. Ablowitz and Y. Zhu. *Phys. Rev. A*, 82:013840, 2010.

[22] C. L. Kane and E. J. Mele Phys. Rev. Lett., 95:146802, 2005.

[23] M.J. Ablowitz. *Nonlinear Dispersive Waves, Asymptotic Analysis and Solitons*. Camb. Univ. Pr., Cambridge, 2011.

[24] A. Szameit and S. Nolte *J. Phys. B: At. Mol. Opt. Phys*, 43:163001, 2010.

[25] C.L. Fefferman, J.P. Thorpe and M.I. Weinstein, "Topologically protected states in one-dimensional systems", arXiv: 1405.4569v1 (2014)